LAL 02-93
November 2002

Overview and status of Calorimetry at LHC

Daniel Fournier

Laboratoire de l'Accélérateur Linéaire

IN2P3/CNRS et Université Paris-Sud - Bât. 200 - BP 34 - 91898 Orsay cedex, France

1 INTRODUCTION

Calorimeters play a central role in "general purpose detectors" for high energy proton-proton colliders, like ATLAS and CMS at the LHC: they allow to trigger, to identify and to measure electrons, photons and jets, as well as escaping neutrinos or other non-interacting particles appearing as missing transverse energy. They also complement muon detection both at the trigger level, and in providing an estimate of the energy lost in traversing them.

Indeed calorimeters are only one part of the experimental set-up, and the overall optimisation of the experiment, i.e. reaching optimal combined performance with the tracker, the magnets and the muon systems was one of the most challenging tasks of the designers.

Today, both ATLAS and CMS calorimeters are well in the construction phase. This is a time when one realises that some choices were indeed wise, when the detector will meet or sometimes exceed the specifications, without having caused too much trouble in the engineering phase. But there are also cases for which compromises had to be made, in order to cope with technical difficulties, budgetary constraints, and schedule.

Taking in turn, electromagnetic, hadronic and forward calorimetry, the talk addresses, for ATLAS and CMS:

- design evolutions since the Technical Design Reports (TDR)
- update of performances (test beam results, simulations)
- systems aspects
- status of construction

At the end, the particular cases of LHCb and ALICE are briefly considered.

2 EM CALORIMETRY

2.1 ATLAS EM Calorimetry

2.1.1 Main features of the design

The ATLAS EM calorimeter uses the Liquid Argon technique, for its excellent stability and radiation resistance, with an "accordion geometry" to allow for hermeticity, speed and high granularity[1]. The barrel part which covers up to $\eta = 1.4$ is separated in two cylindrical "half-barrels", housed in a single cryostat which shares its isolation vacuum with the solenoid (figure 1). Each half-barrel is made of 16 modules and is preceded by a thin presampler layer. In the end-caps (figure 2), each EM wheel (made of 8 modules and covering $1.4 < \eta < 3.2$) is preceded by a thin presampler for $1.5 < \eta < 1.8$.

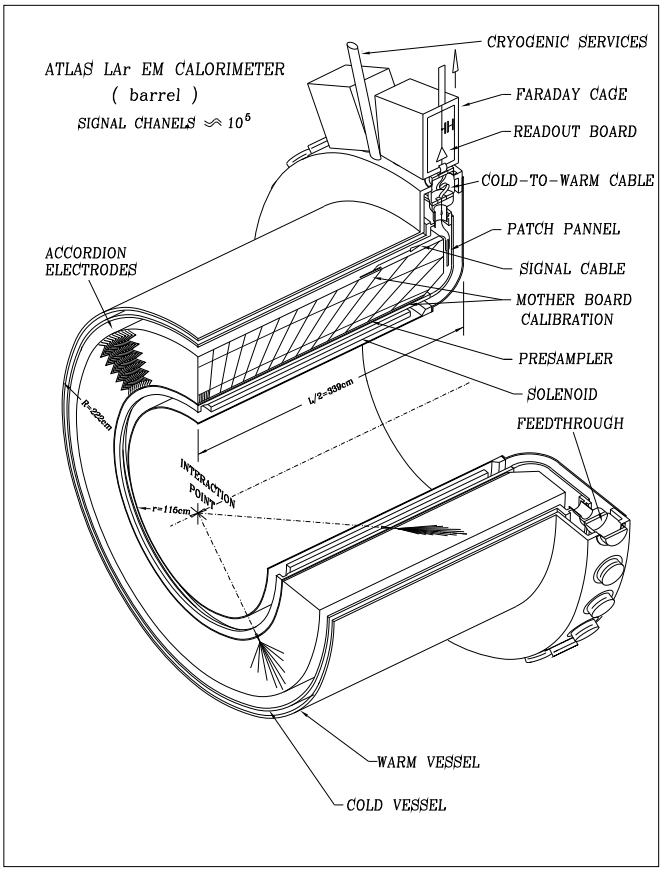

Figure 1: *Sketch of ATLAS EM barrel liquid argon calorimeter (only one half is shown).*

The design energy resolution is $10\%/\sqrt{E}$, with a constant term of 0.7%. The granularity and noise (which was measured in beam tests with ATLAS-like electronics) are as in table 1.

Thanks to the separation in 3 layers in depth, the front strips and central cells allow to measure the direction of photons, independently of the knowledge of the interaction vertex, with an accuracy of 50 mrad$/\sqrt{E}$. The front-end electronics scheme, unchanged since the TDR, features 3 gains (1, 10, 100) shaping amplifiers, analog buffering in SCAs (switch capacitor arrays) every 25 ns, and digitization of a given number of samples (typically 5) upon LVL1 request.

Table 1: *Granularity and noise of ATLAS EM calorimeter.*

Segment	Depth	$\Delta\eta \times \Delta\phi$	Noise (MeV)	Channels	
				barrel	EC
Presampler	1cm Lar	0.025×0.1	40	7808	1536
Strips	$\sim 6X_0$	0.003×0.1	13	57344	27136
Middle	$\sim 16X_0$	0.025×0.025	28	28672	21888
Back	$< 3X_0$	0.050×0.025	23	16384	13184
Total				110208	63744

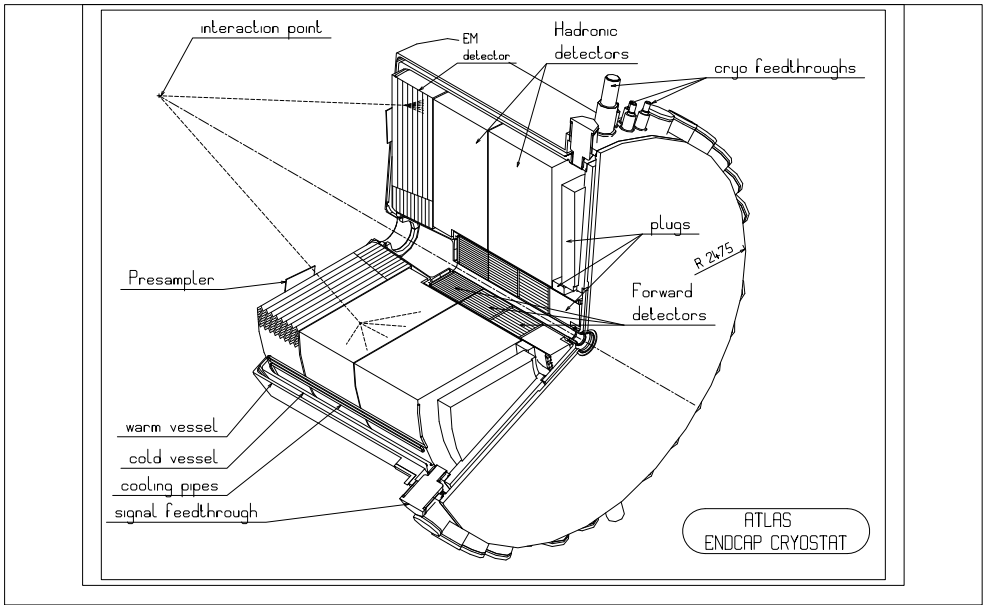

Figure 2: *Sketch of ATLAS end-cap liquid argon calorimeters (one side).*

In this scheme (figure 3), the largest non-saturating gain is first chosen by digitising, in medium gain, the sample closest to the expected signal maximum. Then all samples are digitised with the same gain, allowing then to use digital filtering for combined optimisation of noise and pile-up as a function of luminosity.

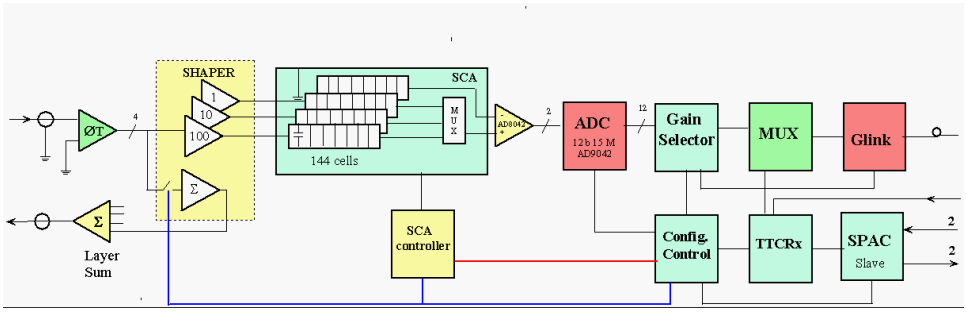

Figure 3: *Simplified readout diagram of liquid argon calorimeters.*

2.1.2 Difficulties with engineering and fabrication

Essentially three difficulties were met:

• Fabrication of large electrodes: In the early prototypes[3], 3-layer, flexible, copper-polyimide electrodes were built with the standard laminates and processing equipment, limited to 60 cm width. Sticking to this approach would have resulted in 7 electrodes to match one absorber, between $\eta = 0$ and $\eta = 1.4$, with the drawback of several thin cracks. It was thus decided, in 1996, to move to 1m width laminates and processing equipment, in order to cover the same area with two electrodes only. It took several years, in collaboration with firms, to reach a satisfactory quality and rate of production. The tuning of non-standard equipment was made more acute due to the presence, on each electrode, of almost 1000 serigraphied resistive pads, necessary to distribute high voltage. The resistances proved rather fragile, in particular when bending electrodes to the desired accordion shape (figure 4). At the time of the conference, more than 75% of the 6000 electrodes of the calorimeter were available.

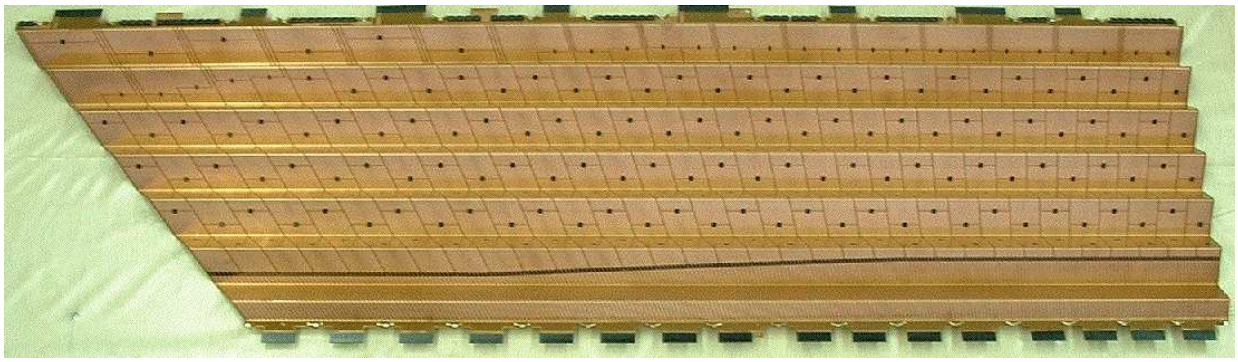

Figure 4: *View of one central barrel electrode ($\eta = 0.0 - 0.8$).*

• HV trouble shooting: Each electrode is kept in its nominal position, in the middle of the gap between two absorbers, using honeycomb bands linked by a set of wires in a sort of net matching the accordion waves (figure 5). The total area of the material used is about 20000 m^2. The nominal high voltage of 1 kV/mm in liquid argon is also used as test voltage in air.

In the early phase of the stacking, done in clean rooms with controlled temperature and humidity, unexpected spurious sparkings, and even some shorts were experienced. A suitable mode of operation could be found only after that a thorough cleaning of honeycomb nets, followed by a specific HV training of each of them was installed.

• Rad hard electronics: The front-end electronics resides in front-end crates, at the high η end of each cryostat, and rather large radius ($\sim$ 2.5 m), where the level of radiations is reduced (10^{12} n/cm^2 and 30 Gy each high luminosity year) and accessibility is possible.

All electronics on these boards was revisited in the last two years such that only radiation-hard processes be used (mostly DMILL). The SCA controller, originally planned in DMILL appeared to have a too low yield. It was redesigned in a 0.25 micron process and is now becoming available.

A set of 30 boards to fill a full front-end crate will be available as of fall 2002, and submitted to detailed tests before series production of boards starts. Most custom designed chips (preamplifiers, shaping amplifiers, SCAs) are already mass produced and being subjected to acceptance tests.

Figure 5: *Close view of the transition between large and small wheel in an EM end cap module, showing the honeycomb nets.*

2.1.3 Test beam results

After thorough tests of "module 0s" in year 1999 and 2000[4], which revealed a few problematic points, later corrected (see below), two series modules of both the barrel and the end-caps were tested in beam in summer 2001 (see dedicated talks to this conference).

The main problem encountered was to understand in detail the behaviour of fast signals (peaking time of 50 ns), in complex structures: from the electrode cell sensing the current signal in the module, to the preamplifier on the front-end board, are: the traces routing the signal (and ground !) out on the electrode, the summing board, the mother board, cold cables, feedthrough and crate baseplane.

Inductances and impedance discontinuities are affecting the physics signal (and the calibration signal injected at the mother board level) propagation, making the electronics calibration to the anticipated level (channel to channel dispersion of 0.25% rms) a more difficult task than anticipated.

Problems were best seen from the scan of a module on constant η or constant ϕ lines: the energy response should be flat, and was not. The results for series modules are now quite good, but one had to:

- improve the ground return on the electrodes,
- re-route the traces on mother boards and summing boards,
- use rather complex formalism to analyse the pulse shapes.

Combining in the same histogram (figure 6) all electrons from the scan of a production module ($\sim$ 600 middle cells) with 245 GeV electrons gives a total resolution of 1.14% which splits more or less equally between the sampling term (0.7%) and the constant term (0.9%). Some corrections, like for the transition between electrodes at $\eta = 0.8$, or correcting some sick electronics channels, are still to be done.

2.2 CMS EM calorimetry

2.2.1 Main features of the design and evolution since TDR

In CMS a $PbWO_4$ crystal calorimeter[5] was chosen for its excellent sampling term of the energy resolution, and for its compactness (the radiation length of $PbWO_4$ is 0.9 cm). R&D concentrated

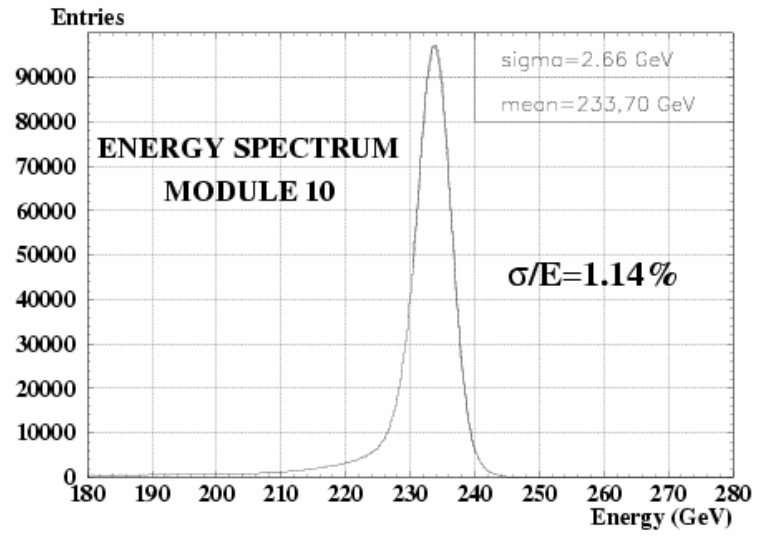

Figure 6: *Combined spectrum of 245 GeV electrons taken over $\simeq$ 600 cells (absolute scale not yet adjusted).*

on purification and controlled doping of the base material, and crystal growth conditions, in order to avoid as much as possible radiation dependent effects. The rather low light yield called for active light converters (APDs, VPTs) which also needed a specific development.

The CMS EM calorimeter consists of two half-barrels, each made of 18 identical modules, and two end-caps each made of two Dees (figure 7). An evolution from the initial proposal, is that now only the end-caps are preceded by a Lead-Silicon preshower.

The sampling term of the energy resolution is thus about $3\%/\sqrt{E}$ for the barrel and $5.5\%/\sqrt{E}$ for the end-caps.

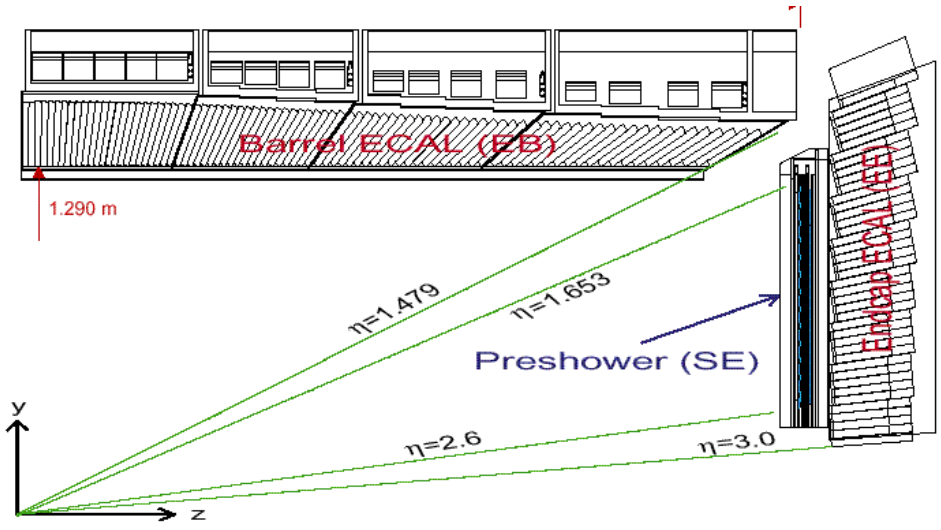

Figure 7: *Geometry of the CMS crystal calorimeter.*

Table 2: *Granularity and channel count of the CMS crystal calorimeter.*

	$\Delta\eta \times \Delta\phi$	Cell size (mm)	Depth (X_0)	Number of channels
Barrel $\eta < 1.48$	0.0175× 0.0175	21.8×21.8	25.8	61200
End-cap $1.48 < \eta < 3.0$	Variable	29.6 × 29.6	23	15632
End-cap preshower		63 × 1.9	3	∼ 130000

2.2.2 Readout and noise

The scintillation light from the crystals which has a broad spectrum around 420 nm, is converted -in the barrel- to an electrical signal by two APDs (25 mm^2 each) glued on the back face of each crystal. In the end-caps, the solenoid magnetic field, almost parallel to the crystal direction, allows the use of 3-stages photo-multipliers (VPTs), less sensitive to radiations than APDs.

A tight Quality Control is applied to the production (see dedicated presentations to this Conference). One of the criteria is a combined crystal-APD efficiency of more than 6 photo-electrons/MeV, measured with a radioactive source (Co^{60}).

The electronics noise depends both on this efficiency, on the APDs "excess noise factor" (∼ 2.2), and on the preamplifier characteristics. The current estimate is around 35 MeV/crystal (this figure is expected to approximately double after 10 years of high luminosity running, because of the shot noise associated to the APDs' leakage current). In the end-caps, read out by Vacuum Photo-Triodes, it is about 50 MeV.

The preamplifier (figure 8) is followed by a 4 gain shaping amplifier (single RC-CR filter with a 43 ns time constant, with gains in the ratio 1, 5, 9, 33). The sample and hold system selects at 40 MHz the largest non saturating gain for digitisation in the fly. This means that the 5 or 7 samples used for a given pulse are, for large signals, taken with different gains. This system is called "floating point preamplifier" since it provides to the downstream stage (ADC) a sampled analogue level, and two bits for the gain.

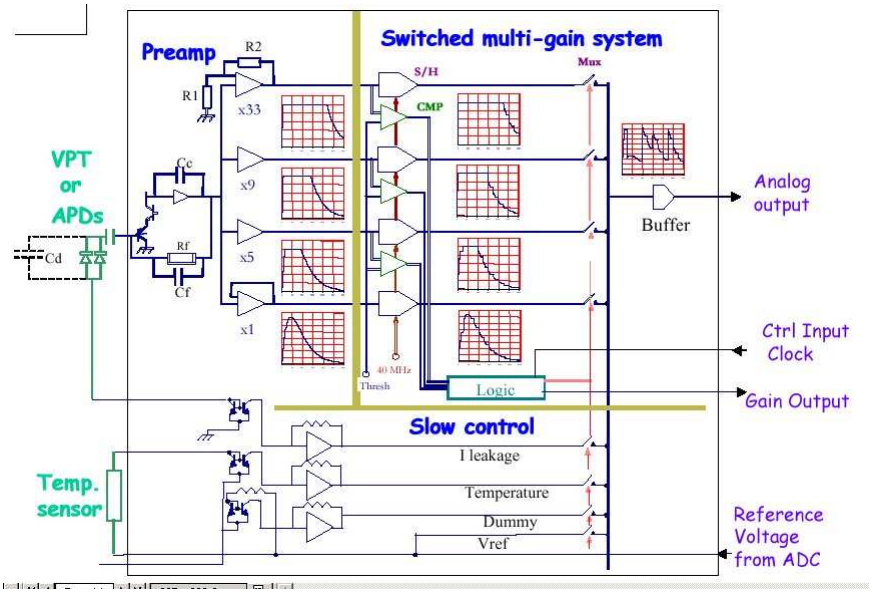

Figure 8: *Simplified diagram of the CMS calorimeter front-end readout.*

Evaluations are still ongoing in the collaboration to decide if all ADC samples are continuously transmitted at 40 MHz (one 1.3 GHz fibre per crystal) for treatment outside of the detector, or if LVL1 primitives (5 x 5 crystals) are formed locally, allowing to output only events (stored locally in a memory) selected by LVL1. The understanding after dedicated talks at the Conference was that the second way is more likely to be chosen, in particular because of financial constraints.

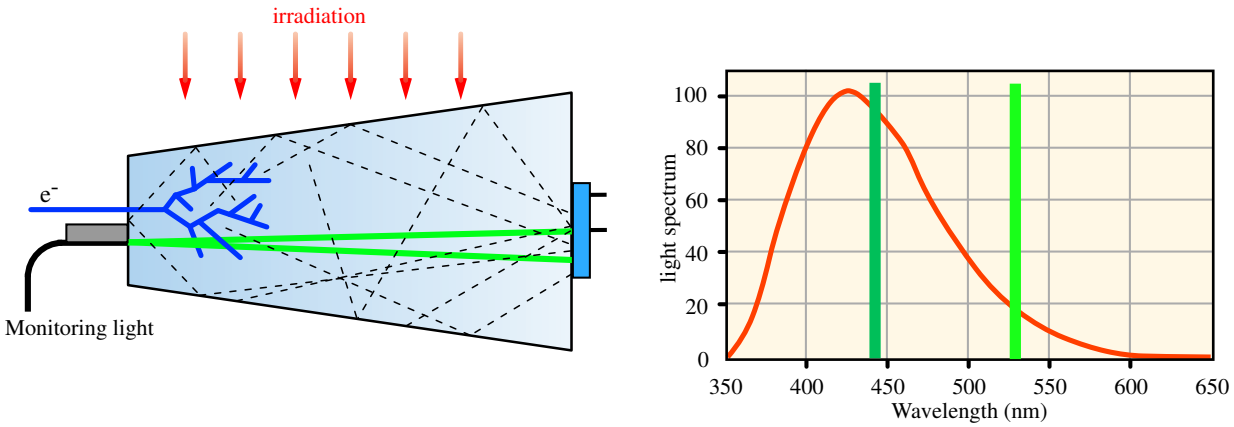

Figure 9: *Geometrical distribution of light, and frequency spectrum.*

2.2.3 Short term follow-up of light output

Exposed to low radiation levels (one Gray per hour or less), like in standard LHC conditions, $PbWO_4$ crystals show a small drop of light output (mostly due to absorption by colour centres), which saturates after a few hours of exposure, and is followed, when irradiation stops, by a recovery with a time constant of typically hours as well (figure 10). In order to limit the consequences of this dependence, the following actions were taken:

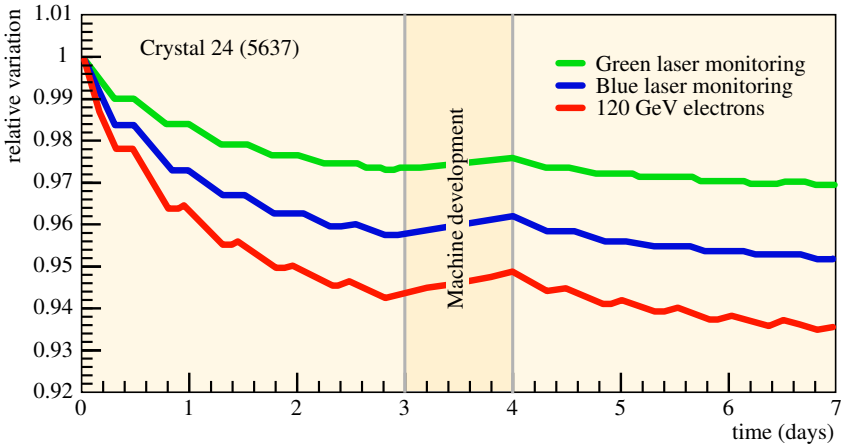

Figure 10: *Simulated behaviour of crystal response to electrons and light pulses (green, blue) as a function of time.*

• Production crystals are requested to vary by less than 6% under exposures like above.

• In order to follow the crystal behaviour at the required pace (hours) during LHC data taking, an optical switching system will send in sequence laser light pulses (at 440 nm) to all crystals of each module.

Because the laser pulses do not have a spectrum identical to the scintillation light, nor the same geometrical distribution in the crystal, the correction cannot be perfect. It was estimated, and confirmed by exposing pre-production modules to test beam[6], that the constant term associated to the residuals of the laser monitoring will not be larger than 0.4%.

2.3 System aspects

While the behaviour of the basic "bricks" of both ATLAS and CMS electromagnetic calorimeters is now well understood, the performance of EM calorimeters as "systems" still critically depends on many integration issues. A selection of the most relevant ones is considered below.

2.3.1 Effect of tracker material and magnetic field

The strong requirements (granularity, speed) on tracking systems has lead to central tracking detectors which are unfortunately rather massive, as illustrated by the CMS case in figure 11[7] (ATLAS is similar)[8]:

Electrons and photons are thus subject to early showering in the tracker (plus solenoid and cryostat in the case of ATLAS) before reaching the active calorimeter (or presampler) medium.

The low energy calorimeter tail subsequently generated is particularly visible in CMS due to its better energy resolution, and larger magnetic field (4T for CMS, 2T for ATLAS). Figure 11 shows the energy spectrum of electrons after that an isolation criterium is applied at the trigger level (adding a 6% inefficiency), and reconstructing the shower with an "hybrid cluster" (i.e. extended to sub-clusters in the azimuthal direction).

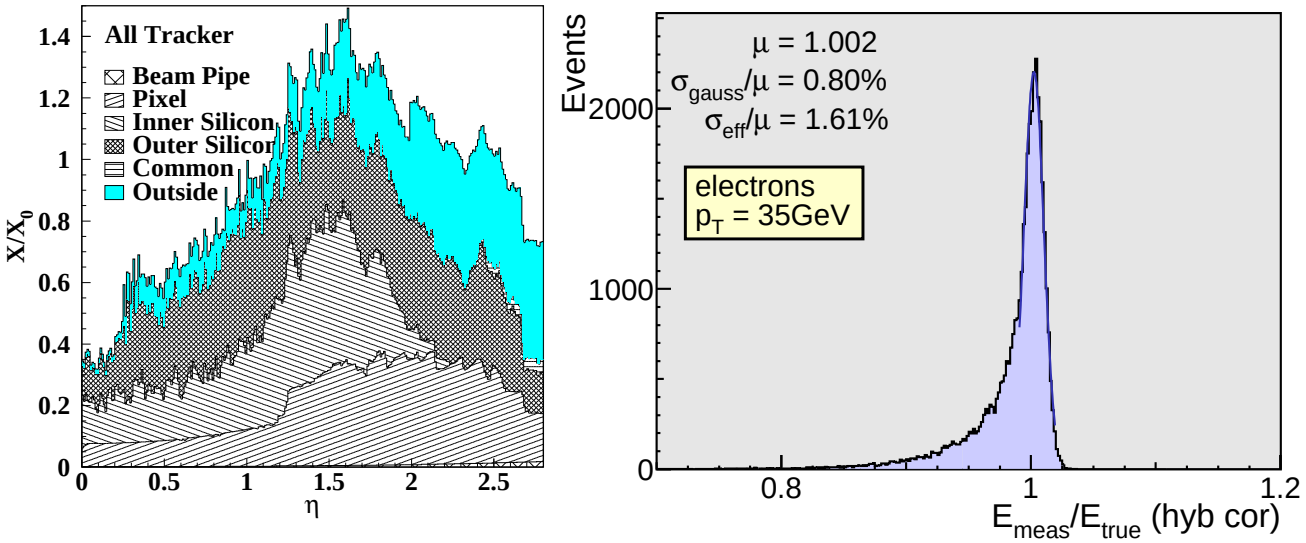

(a) (b)

Figure 11: *(a): Material in the CMS tracker; (b)Simulated electron energy spectrum (normalised to true energy) in the CMS detector.*

In the same conditions, for 35 GeV E_T, the position resolution, converted to angular resolution assuming a fixed vertex is about 1.0 mrad in η and 2.1 mrad in ϕ. For comparison, with the middle sampling of ATLAS the corresponding figures are 1.0 and 1.5 mrad respectively. Once more the worse resolution in azimuth is to be associated with the effect of bremsstrahlung.

Photons which do not interact before a radius of ~90 cm are much less affected than electrons. In CMS, for a 110 GeV Higgs decaying into $\gamma\gamma$, 78% of the reconstructed masses without conversion fall in a 1.9 GeV mass bin. However, the efficiency of the "non-converting" photon cut alone is about 70% per leg. In ATLAS using both interacting and non-interacting photons the 80% acceptance mass bin is 3.1 GeV wide. The comparative performances of the two experiments for $H \rightarrow \gamma\gamma$ detection depend on the resolution that CMS will reach with the converted photons, and on several other aspects (background rejection, pointing - see below).

2.3.2 Calibration in situ

In ATLAS it is assumed (and now confirmed by beam test of series modules) that the detector is uniform "by construction" to better than 0.4% rms in areas of $\Delta\eta \times \Delta\phi = 0.2 \times 0.4$ or larger. Taking this as "minimal hypothesis", there would be 440 areas (0.2×0.4) to be intercalibrated in situ. It was shown by simulations[9] that imposing the Z mass constraint to $Z \rightarrow e^+e^-$ decays measured in the calorimeter only (i.e. without reference to tracking information) an adequate inter-calibration (0.3% rms cell to cell dispersion) can be obtained with data recorded during 48 hours at low luminosity (where the rate of $Z \rightarrow e^+e^-$ is about 1 Hz). The same constraint gives indeed an extremely precise absolute energy scale calibration.

In CMS the crystals are first calibrated in the laboratory with laser pulses and/or radioactive sources. Experience shows that the correlation of this calibration with the response to high energy electrons from beam tests is not better than 6% rms. In the likely case that all crystals cannot be calibrated in test beam, the in-situ inter-calibration will use lab results as starting point. The currently developed strategy is based on using electrons from W decays, measured with the tracker. This is better adapted than the Z mass constraint, due to the higher rate. Preliminary studies[10] indicate that two months of low luminosity data are necessary to intercalibrate to 0.5% rms in this way. When this is done, Z decays give the absolute energy scale. Considerations on azimuthal uniformity of response to minimum bias events may help in this inter-calibration task.

2.3.3 Constant term

Besides the residual of the crystals or cells inter-calibration, and of short term variations, like the crystal output light depending on recent irradiation history, there are several contributions to the constant term. One of them is associated with temperature dependence of signal response:

• the temperature dependence of the liquid argon signals was measured to be $-2\%/^0$K (see ref 1, chapII, p.33). The liquid argon bath is subject to free convection, which can be turbulent in some places despite the small gradients (the viscosity of argon is very low), and is therefore difficult to simulate. The total heat influx is about 2.5 kW per cryostat. Extensive finite elements simulations (preliminary) indicate an overall temperature dispersion within the barrel sensitive volume of ± 0.15 degrees, hopefully small enough to avoid the need for corrections. In case of larger gradients, corrections will be possible offline, thanks to continuous recording of ~300 precision temperature probes located at the surface of modules.

• In CMS the temperature dependence of "crystal+APD" is about -4.3%/^{0}K. Removing the heat dissipated by front-end electronics (2 W per channel, i.e. 160 kW in total) right in the back of the crystals, while keeping an excellent temperature uniformity, is a challenge. A thermal analysis of the crystal calorimeter was made, based on the use of pressurised water circulating in a dense pipe network, separated in three layers, each layer being isolated from the more external one by thermal shields. As a result, it is estimated that a temperature dispersion of $\pm$ 0.05^{0}K within the crystal volume can be reached.

Overall, ATLAS claims a constant term in the energy resolution of 0.7%, and CMS of 0.55%. At this stage it might be useful to stress that those figures will only be reached if processing key physics channels (W$\rightarrow$ eν, Z$\rightarrow$ ee) is easy, with a fast turn-over, as of LHC start-up.

2.3.4 Use of granularity

Background rejection: In the search for the Higgs in two photons (up to 150 GeV) it is necessary to bring the background from jet-jet and γ-jet events well below the irreducible $\gamma\gamma$ background. After standard shape cuts the remaining background is dominated by jets fragmenting to single π^0s. Using the high granularity of the calorimeters the performances reported in table 3 were obtained by simulation, at 50 GeV E_T.

Somewhat inferior in the barrel, CMS is equivalent or slightly better in the end-caps,thanks to the high granularity of its lead-silicon preshower.

Table 3: *π^0rejection in ATLAS and CMS, for ~80% photon efficiency.*

	0-0.45	0.45-1.	1.-1.5	~1.7	~2.4
ATLAS(all γ)	3.6	3.1	2.6	3.1	2.8
CMS (unconverted)	3	2.2	2	3.5	2.5

Pointing: The measurement of the direction of non-converted photons is a unique feature of ATLAS (indeed measuring the direction of converted photons is easy in both detectors). Such direction measurements are important in several cases, in particular for Higgs decaying in two photons, where the direction error contributes to the mass resolution (at high luminosity, the interaction vertex is often ambiguous for $\gamma\gamma$ events). Gauge Mediated Susy Breaking models, in which the neutralino $\rightarrow$ photon-gravitino decay may have a long enough life time to produce "non-pointing photons", which can be used to sign the process, is another example where pointing is useful.

2.3.5 Linearity

Excellent linearity is required for precision physics. One topic particularly demanding is an improved measurement of the W mass using the W $\rightarrow$ eν channel.

Illustrated below is the linearity observed in one of the best calorimeters built so far, namely the homogeneous krypton Calorimeter of the NA48 CP Violation experiment at CERN[11] (figure 12). Over the energy range of interest for this experiment, the systematic uncertainty was estimated to be 6 10^{-4} rms. What would be needed to meet the W mass measurement requirement (25 MeV error, overall) is gaining a factor of 3, however on a restricted range ($M_Z/2$ to $M_W/2$). This would probably be possible with the NA48 calorimeter,... but ATLAS and CMS calorimeters are more complex devices, and not much was done so far to assess them, in this respect, at the required level.

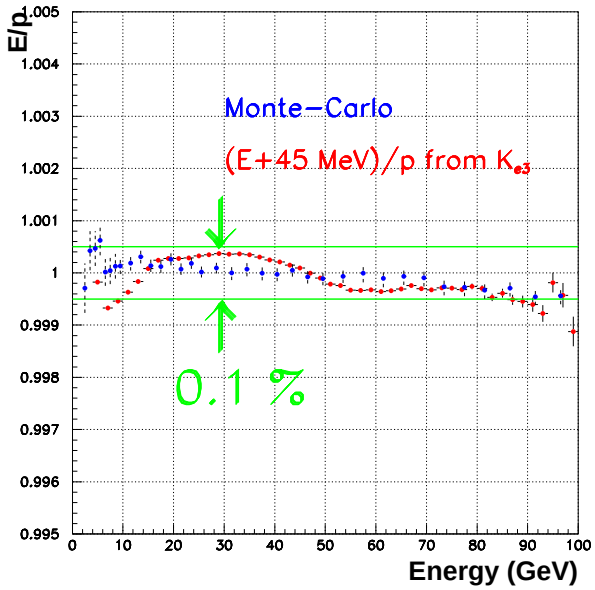

Figure 12: *Ratio of electron energy, measured with the krypton calorimeter, and momentum from the magnetic spectrometer, in NA48.*

2.3.6 Data reduction

Large number of cells, large dynamic range, and high trigger rates produce very large amount of data (∼1.0 Mbyte/event for the calorimeter itself, in both experiments). The associated cost for storing and processing these data was recently put under scrutiny[12], which triggered some further dedicated work in the collaborations.

One route for data reduction being explored by both ATLAS and CMS, is "zero suppression". While at first sight cutting cells containing "only noise" is rather tempting, this may generate subtle adverse effects on precision physics, difficult to resolve later on. Detailed Monte Carlo evaluations (and control samples) will be needed before such a data reduction can be implemented at the "on line" level, but prospects are interesting[13].

3 HADRONIC CALORIMETRY

All the electromagnetic component of jets, plus a fraction of the charged hadronic part, is deposited in EM calorimeters representing 1 to 1.5 interaction length λ. EM calorimeters being calibrated with electrons, the energy measured for jets has to be converted to "hadronic scale" when, as it is the case for ATLAS and CMS the electron to hadron ratio (e/h) is larger than 1.

To catch the remaining part of jets, more massive devices are needed, the "hadronic calorimeters", up to a total thickness of $\sim 9\lambda$ or more. Full coverage in pseudo rapidity is mandatory, up to $\eta \simeq 5$.

The instrumentation of the most forward region ($3 < \eta < 5$) raised specific problems. This part is considered in the next section.

3.1 CMS hadronic Calorimeter

CMS uses scintillator sampling calorimetry both in the barrel and in the end-caps (up to $\eta = 3.0$)[14].

The choice to place the full calorimeter inside the coil imposed a non magnetic absorber (brass, in plates of 5cm). The constraint of the coil size (inner radius = 2.95 m, outer radius =3.80m) in practice limited the total thickness at η =0 to 7 λ. In order to improve on this figure, it was found necessary to add a "tail catcher" behind the solenoid coil, for a total of 9.4 λ, compromising to some extend-in a limited pseudo rapidity range-the original design criterium.

Scintillator tiles (3.7 mm thick) inserted in between the brass plates, are readout by wave length shifting fibres, fitted in grooves. The former are glued to clear fibres which bring light out of the solenoid, up to Hybrid-Photo-Detectors (proximity focused single stage photomultipliers with "pixelised" silicon diode target) able to work in the fringe magnetic field. The light yield is about 10 pe/GeV.

The granularity is 0.087 × 0.087 (5× 5 EM towers) with 3 samplings in depth, the first one being rather thin in order to sample the particles coming out from the ECAL.

Close to the upper (η=3) boundary, the cumulated radiations (3 10^4 Gy integrated over 10 years) will start to affect the collected light (mostly because of a reduction of the WLS fibre absorption length). This will be monitored by a moving source, and using LHC data itself.

3.2 ATLAS Tile Calorimeter

ATLAS uses scintillator sampling calorimetry in the barrel and in the extended barrel, up to η = 1.7[15].

The iron plates (5mm thick, grouped by 3) and scintillator plates (3mm thick), are perpendicular to the beam axis. The thickness up to the last active layer is 9 λ at η=0.

The scintillation light is collected by WLS fibres running on either side of scintillator plates. This allows a rather easy bundling of fibres to form towers, read out by photomultipliers located in the "girders" (outer radius = 4.23 m). At this place the solenoid and toroid fringe fields are low, and further reduced by shielding with high permeability metal sheets.The light yield is about 40 pe/GeV.

The granularity is 0.1 × 0.1 (4 × 4 EM towers) with 3 samplings in depth (the last segment has a granularity of 0.2× 0.1). Towers are pointing in azimuth, and pseudo pointing in η.

3.3 ATLAS Hadronic End-Cap

Beyond η = 1.5, ATLAS uses the Copper-Liquid Argon technique[1]. Among other aspects this alleviates radiation resistance problems. The detector consists of two wheels-HEC1 and HEC2- in the same cryostat as the Electromagnetic end-cap and Forward calorimeters (see figure 2).

The copper plates (25 mm thick in HEC1, 50 mm in HEC2) are perpendicular to the beam axis and interleaved with 4-uple liquid argon gaps in a configuration of electrostatic transformer. Pairs of adjacent cells in depth are connected to a preamplifier located in the liquid, at the periphery of the wheels. Summing of signals to form readout towers is done downstream of the preamplifiers, in the cold as well. This scheme gives adequate speed of response, with signal rise-time of $\simeq 50ns$.

The granularity is 0.1 × 0.1 (4 × 4 EM towers) up to η = 2.5 and 0.2× 0.2 up to η = 3.2, with 4 samplings in depth (at the time of the TDR, the two segments of HEC2 were ganged together).

3.4 Resolution, linearity

Prototypes of the hadronic calorimeters briefly described above have been tested in high energy pion beams, both in "standalone" mode, and with their EM counterpart in front.

In all cases the electron to hadron response ratio (e/h)is greater than 1, both in the electromagnetic and hadronic compartments, which affects both the linearity and the constant term. The example of the CMS calorimeter[16] is summarised in figure 13. With a suitable weighting, depending on signal

height on an event by event basis, the combination crystal calorimeter-hadronic calorimeter can be made nearly as good as the hadronic part in stand alone.

Results from the ATLAS combined LAr-Tile prototypes[17] show a similar behaviour, as given in figure 14. Cell by cell weighting (a la H1) improves by $\sim$ 15% the resolution of the "benchmark" method, with a single weight per compartment.

Performances have also been extrapolated to jets at LHC. A larger cone size improves the sampling and constant terms of the energy resolution, but the fluctuations of the noise and pile-up soon become dominant. Cone sizes down to 0.4 are used for the high luminosity case. Some relevant parameters are summarised in table 4 (the pile-up is the expected value at nominal high luminosity in a cone ΔR=0.7).

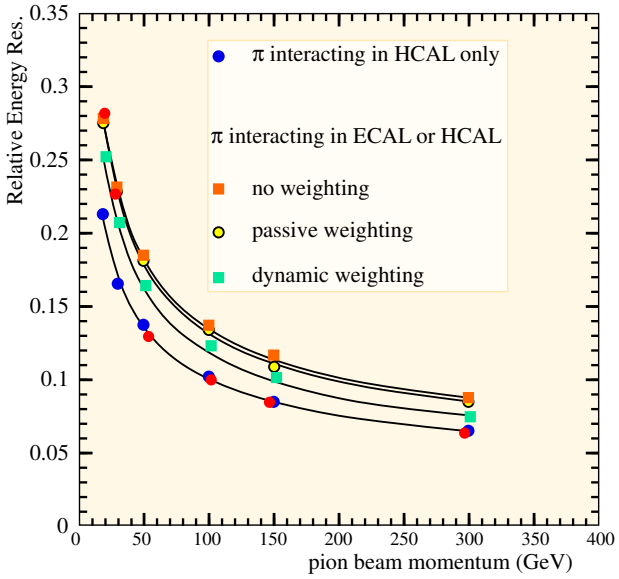

Figure 13: *Pion resolution with prototypes of the CMS calorimeter.*

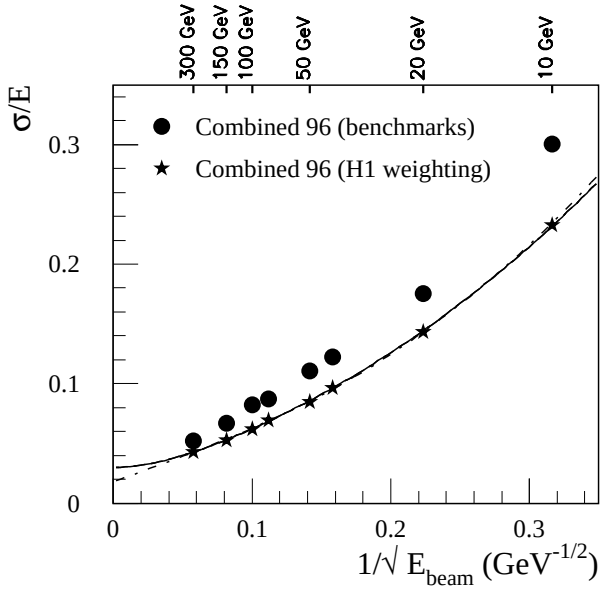

Figure 14: *Pion resolution with prototypes of the ATLAS calorimeter.*

Table 4: *Performances of ATLAS and CMS hadronic calorimeters*

		CMS standalone	CMS combined	ATLAS Tile	ATLAS combined	HEC standalone
Pions	e/h had	$\sim$ 1.4		1.30 $\pm$ 0.01	1.37 $\pm$ 0.01	1.47 $\pm$ 0.04
	e/h EM		$\sim$1.6		$\sim$1.7	
	sampling	$100\%\sqrt{E}$	$110\%\sqrt{E}$	$52\%\sqrt{E}$	$70\%\sqrt{E}$	$75\%\sqrt{E}$
	constant		5%	3.0%	3.3%	5.0%
	noise	small	$\sim$ 1 GeV	Small$\sim$0.5 GeV	1.8 GeV	5 GeV
Jets ΔR = 0.7	Sampling	110%		53%		64%
	Constant	5%		3%		3.6%
	Noise $\oplus$ Pile-up	13 GeV E_T		14 GeV E_T		

Attempts are being made in CMS to improve the jet resolution by using the tracker information[18], on the basis of what was done, with some success, in some LEP experiments and elsewhere. The so-called "energy flow" approach consists mainly in replacing the energy of each somewhat isolated charged hadron measured in the calorimeter, and linked to a track, by the corresponding momentum measured in the tracker. As an example, the energy resolution of 100 GeV jets is improved from

12 to 8 GeV (simulation done in a low luminosity case). While this looks promising, systematic effects associated to the method need to be evaluated case by case, depending on the physics analysis undertaken.

3.5 In situ Calibration

• Z+jet: Given its cleanliness and high cross-section, this channel is particularly attractive to calibrate jets to the lepton scale of selected Z decays, by transverse momentum balance. ATLAS simulations showed that, with a veto on extra jets and/or an alignment cut in the transverse plane ($\Delta\phi$ cut), the energy bias can be kept at the few % level [9] (see figure 15).

The method is also suitable to calibrate b-jets (tagged with a displaced vertex), and forward jets by selecting events with the jet in the forward direction, while the leptons of the Z are kept central.

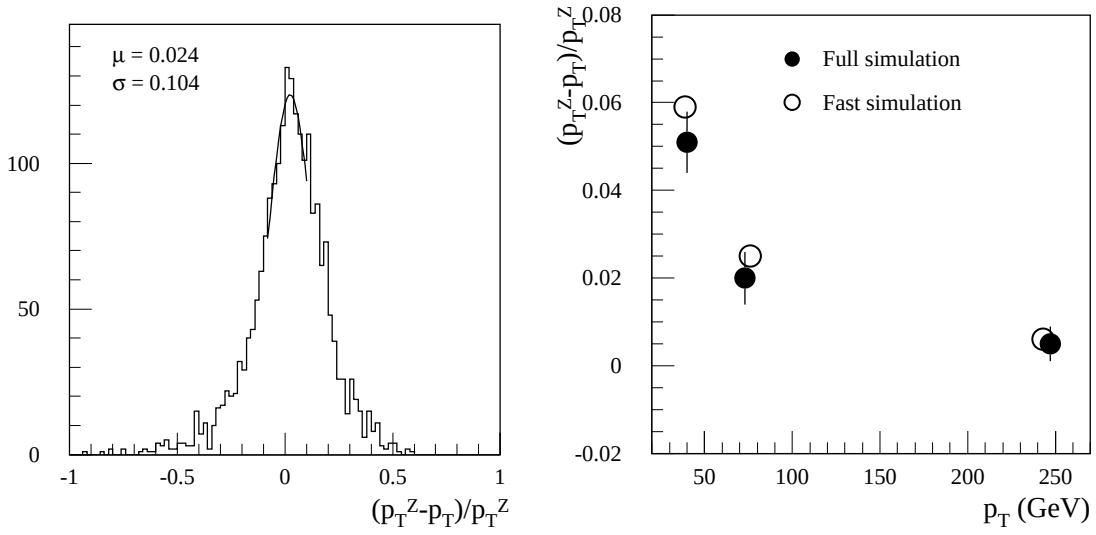

Figure 15: *Jet calibration with Z + jets events. Left: relative p⊥ difference between Z and jet, for p⊥ > 40 GeV. Right: evolution of the average fractional imbalance with p⊥ jet.*

• The other main tool consists in imposing the W mass constraint to W $\rightarrow$ jet-jet decays suitably selected. This method is particularly well adapted to top mass measurements, using the event sample itself.

3.6 Some illustrations

To illustrate the methods briefly described above, a selected sample of results obtained in ATLAS by simulation[19] are shown below:

• Measurement of the top mass: It is presently estimated that, with the statistics of one year at low luminosity (10 fb^{-1}) the systematic error on the top mass measurement, using the 3-jets decay mode, can be brought down to 1% (figure 16).

• Higgs associate production: The discovery of a Higgs boson above the LEP exclusion limit, up to $\simeq$ 130 GeV will be difficult at LHC and requires several modes. The associated t-$\bar{\text{t}}$ H, H $\rightarrow$b $\bar{\text{b}}$ mode can usefully complement H$\rightarrow \gamma\gamma$ if the two b-jet mass resolution is good enough, and the background well understood. A simulated spectrum, with signal (120 GeV) and background is shown in figure 17.

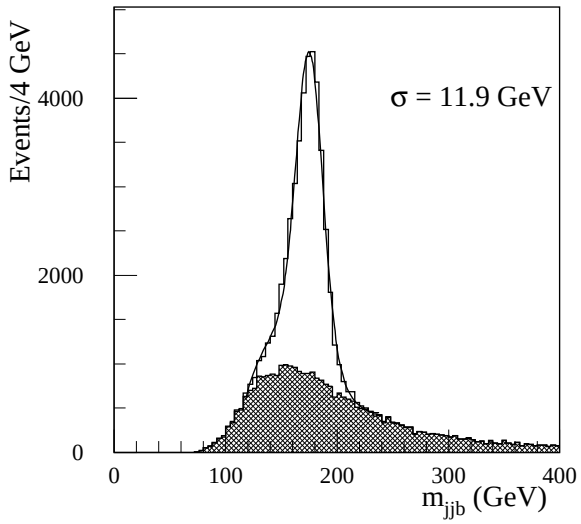

Figure 16: *Invariant jjb mass from top decays (10 fb^{-1} integrated luminosity). The background (shaded) is dominated by "wrong combinations".*

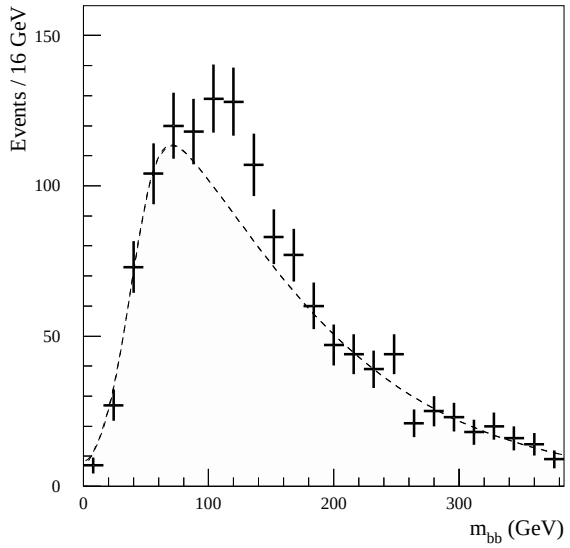

Figure 17: *Invariant mass of tagged b-jets pairs, above background, for associate $t\bar{t}H$ production and 100 fb^{-1} integrated luminosity.*

4 FORWARD CALORIMETRY

4.1 A harsh region

The first "raison d'être" of forward calorimetry is to avoid tails due to particles escaping around the beam pipe, in the measurement of missing E_T. For practical reasons, it is difficult to instrument beyond η =5. This is in general adequate, although some channels where precise measurement of E_T is necessary would benefit from an extended coverage (H$\rightarrow \tau\tau$ at low luminosity is such an example).

At shower max and $\eta = 4$, in ATLAS, the neutron flux is about 3 10^{15}n/cm^2/year, a factor 1000 above the barrel EM situation. The main constraint in designing these devices was thus their survival

to 10 years of high luminosity. Enough granularity at high pseudorapidity is necessary in order that the relative precision on jet direction do not spoil the relative energy resolution.

A summary of specifications and general parameters, for ATLAS and CMS, is given in table 5 below:

Table 5: *Parameters of ATLAS and CMS Forward Calorimeters.*

	ATLAS	CMS
Technique	Tungsten-Liquid Argon	iron-quartz fibres
Geom acceptance	$3.1 < \eta < 4.9$	$3.0 < \eta < 5.0$
Layers in depth	3	2
Number of channels	1792/side	2096/side
Sampling term	$90\%/\sqrt{E}$	$200\%/\sqrt{E}$
Constant term	8%	~10%
Noise + pile-up *	~ 6 GeV E_T	~ 6 GeV E_T

* in $\Delta R = 0.4$ at high luminosity

4.2 The CMS Hadronic Forward Calorimeter

CMS chose to recess the front face of their hadronic Forward Calorimeter (HF) at 11m from the collision point and to base the detection on Cerenkov light produced in quartz fibres embedded in a metal matrix (figure 18), with a pitch of 2.5 × 2.5 mm [20].

This approach samples mostly the neutral component of the shower, and thus features a large e/h ratio. The detector sensitivity is $\leq$ 1 pe/GeV.

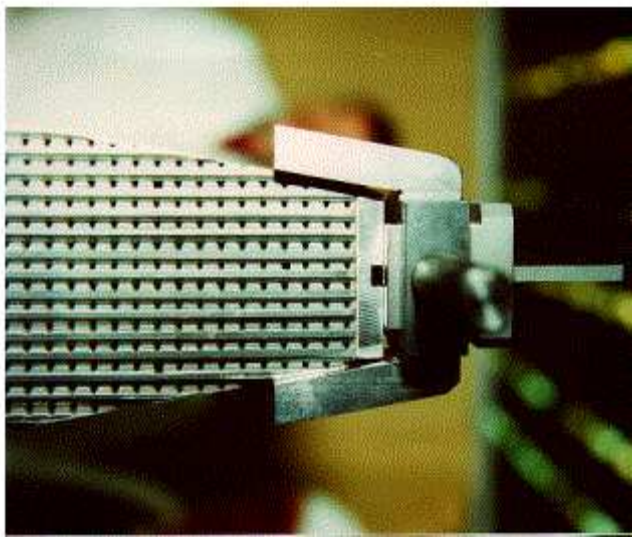

Figure 18: *Central part of a CMS HF module, prior to fibre insertion.*

Despite the high radiation tolerance of quartz it is expected that the light from the most central part of the device will be reduced by ~30% after 10 years at high luminosity, this being mostly due to an effect on the fibre cladding (figure 19).

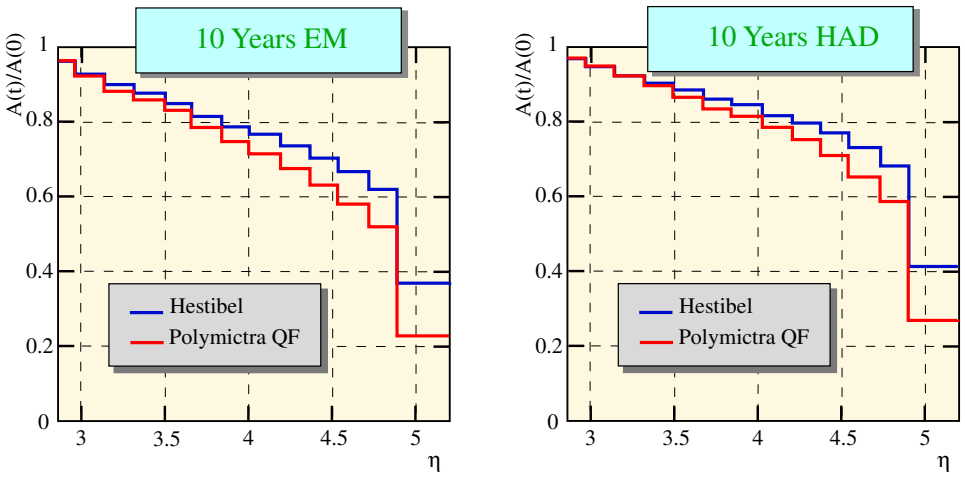

Figure 19: *Simulation of radiation damage on light yield from fibres of the CMS HF.*

4.3 The ATLAS FCAL

The choice of ATLAS was to integrate the forward calorimeter in the same cryostat as the EMEC and HEC calorimeters. The structure chosen is a metal matrix with holes parallel to the beam axis, in which tubes with rods are inserted (figure 20).

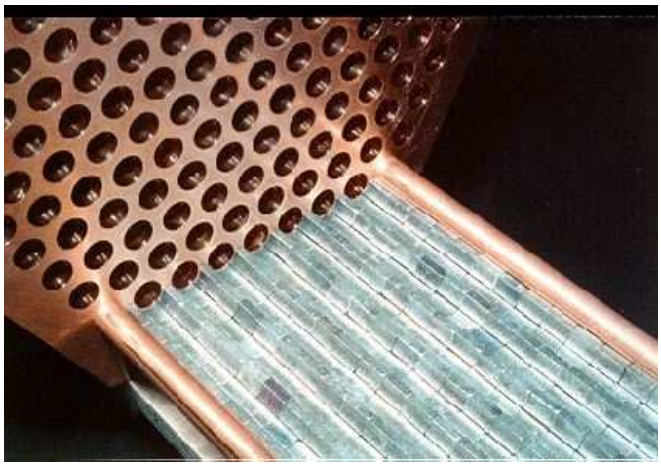

Figure 20: *Structure of the ATLAS Forward Calorimeter.*

To avoid spill-out of showers, a dense calorimeter was mandatory, which dictated the use of Tungsten for the hadronic part (average density is 14 g/cm^3). Radiation resistance of liquid argon made the device possible, even with its front face at 4.7 m from the collision point.

The other adverse effect due to the high rates is space charge build-up. The tolerable flux goes like $V^2/d^4\mu$ (μ is the ion mobility) and calls for extremely thin gaps. ATLAS chose d=250 microns in the first (EM) section and 375 microns downstream.

Several prototypes demonstrated the soundness and expected level of performance of this concept (see ref 9, section 5.1.4). However the price to pay is an extreme cleanliness in assembling the device, in order to prevent being plagued by high voltage problems (here high voltage is only 300 volts !).

4.4 Forward jet tagging

Jet tagging in the forward direction opens up the possibility to select samples of final states (Higgs boson) produced by WW or ZZ fusion, for which the signal to background ratio is more favorable than in inclusive reactions.

The main acceptance region is between $\eta = 2$ and $\eta = 4$ (see figure 21), which underlines the necessity to optimize the transition near η=3 between the "end-cap" part and the "forward" part.

As an example qqH $\rightarrow$qqWW $\rightarrow$ lνlν jet-jet was studied by simulation in ATLAS. It was shown that requiring a double tag reduces the effect of fake tags to manageable effects (-10% relative loss on double tag efficiency -E$\perp$> 15 GeV- due to a cell cut at 1 GeV E_T), even at the nominal high luminosity.

5 STATUS OF CONSTRUCTION

5.1 Construction advancement

The construction of all parts of ATLAS and CMS calorimetry is now going "full speed".

There is however a rather large spread in the present degree of completeness, as a result of several factors, including:

- the amount of R&D which had to be carried out
- the difficulties in transferring techniques from labs to industry
- the profile of available money and man-power
- the overall integration and installation plan of the experiment.

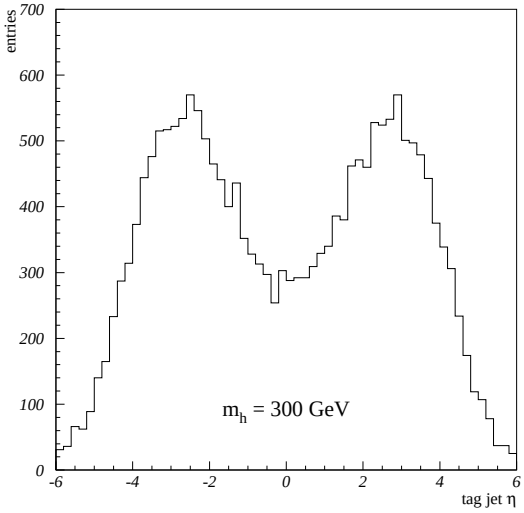

Figure 21: *Pseudorapidity distribution of forward jets,in the production of a 300 GeV Higgs boson by WW fusion.*

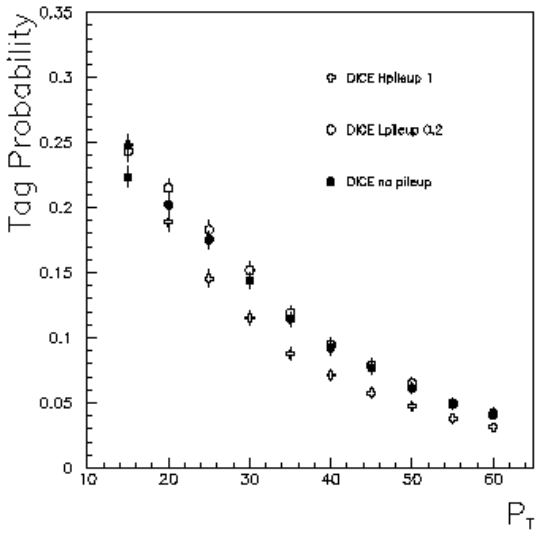

Figure 22: *Effect of pile-up on the double-tag efficiency.*

In particular the CMS cavern shall be available later than the ATLAS one, and thus installation in the pit is taking place later (in 05 and 06), with large elements being assembled in advance in the

dedicated large surface hall. As an illustration the state of advance of ATLAS production is given below (table 6), for a global detector commissioning as of oct 06 .

Table 6: *Status of production and integration of ATLAS Calorimeters in spring 02.*

		Main Components procured	Module assembled	Integration on surface ends		Installation in pit
ATLAS	EM-barrel	80%	30%	Apr 04		July 04
	EM-EC	80%	25%	ECC	July 04	Nov 04
	Tile	90%	75%			
	HEC	90%	70%	ECA	Nov 04	March 05
	FCAL	70%	40%			

5.2 Staging plans

Being so critical for the experiment performance, and central in the installation sequence, calorimeters have been so far protected against staging or descoping plans, which may however at some stage affect some back-end electronics.

Many beautiful and impressive pictures were shown during the Conference. A few of them are selected below.

5.3 Some ATLAS pictures

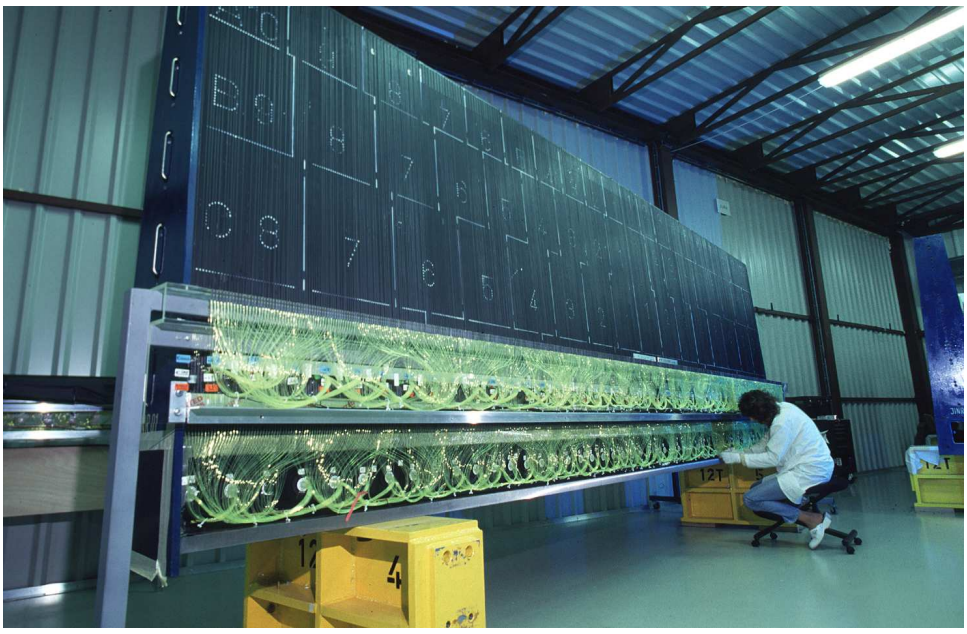

Figure 23: *Work on optical fibres in the first Tile barrel module.*

Figure 24: *Full body of the first hadronic section of the FCAL.*

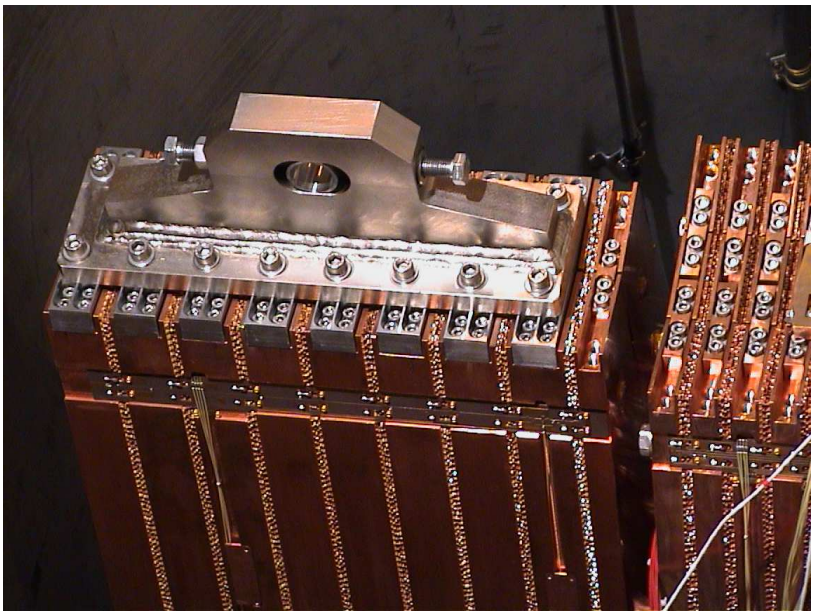

Figure 25: *HEC modules in their test cryostat.*

Figure 26: *EM barrel modules ready for first half-barrel assembly.*

5.4 Some CMS pictures

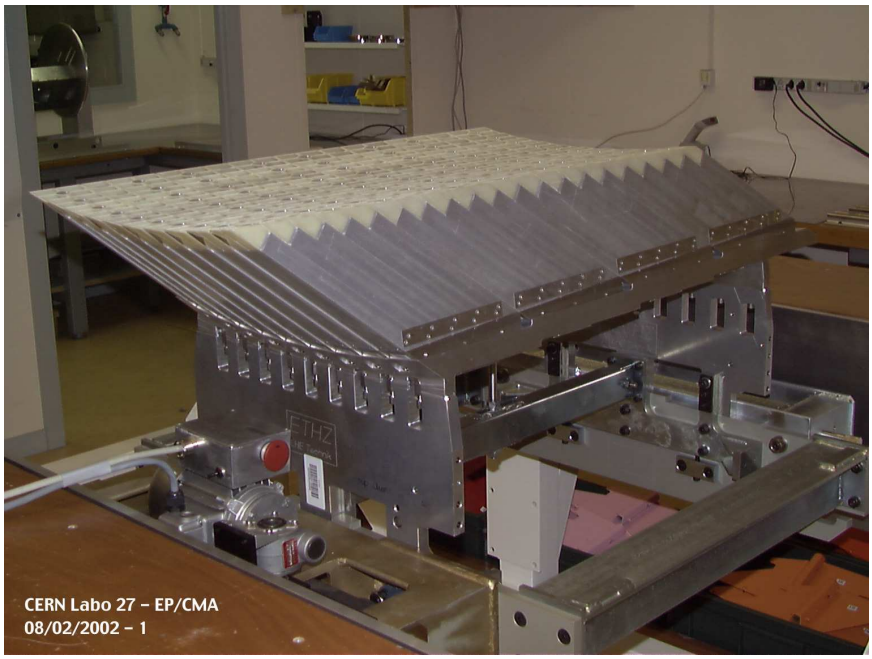

Figure 27: *Assembly of first ECAL submodule at CERN.*

Figure 28: *Starting assembly of hadronic forward part.*

Figure 29: *Trial assembly of hadronic barrel part.*

Figure 30: *Hadronic barrel modules stored at CERN.*

6 CALORIMETRY IN LHCb

6.1 General strategy

LHCb detection is concentrated in a 250 mrad half-angle forward cone around the beam axis ($\eta \geq 2$), which optimises the ratio of event rate to coverage for B physics[22].

The aim is to have at the collision point a luminosity which maximises the number of bunch crossings with a single proton-proton inelastic interaction. In order to go fully in the direction of "clean events", the calorimeter pulse shaping/clipping is made such that signals generated by collisions in the preceding or the following bunch crossings, are negligible at the time of the main bunch crossing.

The experiment aims also at using B decay modes with π^0 and $\eta^0 \rightarrow \gamma\gamma$ in the final state.

6.2 LHCb layout

The LHCb calorimeter system consists of:

- A scintillator pad detector (6000 pads)
- A preshower detector (scintillator pads after $3X_0$ of lead)
- A "shashlik" EM calorimeter (6000 towers)
- An ATLAS like "Tile" hadronic calorimeter (1500 towers)

6.3 Some performances

The energy range of the calorimeters is limited to $\simeq$ 300 GeV and can be covered by a single electronics gain of 12 bits dynamic. EM calorimeter and pad/preshower cells have a transverse size of 4x4 cm in the central part, 8x8 cm in the middle part, and 16x16 cm in the outer part, giving a total transverse size of about 6.5x6.5 m. All devices are read out by photomultipliers (multi anodes for the pad and preshower detectors).

The pion/electron rejection provided by the pad-preshower system is around 12 between 10 and 50 GeV. This complements the rejection from the combined magnetic and calorimetric energy measurements (E/p). Expected energy resolutions are $10\%/\sqrt{E}$ and $80\%/\sqrt{E}$ for the EM and hadronic part respectively.

6.4 A worry: scintillator damage by radiations

The central part of the calorimeter will see doses, integrated over several years of running, in the Mrad range (several 10^4 Gy), which will induce light losses. It was estimated that residuals in the correction of this effect will lead to an increase of the constant term of the EM energy resolution from 0.5% to 1.5%. If things go to the worse, the central part could be replaced after some running time.

7 CALORIMETRY IN ALICE

The Alice experiment at the LHC is dedicated to ion-ion and proton-ion collisions[23].

7.1 Photons at large angle

The EM PHOS calorimeter[24] is optimised to measure direct photons, π^0 and η^0 between 0.5 and 10 GeV/c. Since only single spectra and correlations are looked for, a complete coverage is not mandatory. The chosen detector covers 100^0 in azimuth and $\pm$ 0.12 in rapidity. It is located at 4.6 m from the beam axis. Alice chose $PbWO_4$ crystals, used in a very similar way to CMS. Crystals have a transverse size of 22$\times$22 mm and are read out by APDs. In total, there are 17280 crystals in the detector.

7.2 Zero degree calorimeters

Zero degree calorimeters play the special role, in heavy ion collisions, of detecting neutrons and protons from nuclear break-up of the incident ions.

In a symmetric machine like LHC, the neutron spot has a 1 cm^2 size, in between the two rings, 120 m away from the interaction point. Protons are bent away by the beam elements and fall on either side of the beam pipes.

In these conditions, compactness and radiation resistance are the prime requirements.

Alice has chosen quartz fibres embedded in a Tantalum matrix for neutrons, and in a brass matrix for protons[25]. These detectors are extrapolation of what was used in the heavy ion experiment NA50 at the CERN SPS where an energy resolution of 5.4% was observed when sending 33 TeV lead ions in a similar calorimeter.

8 SUMMARY

• In many-if not all-cases ATLAS and CMS made different calorimetry choices: this is a safety for the LHC physics programme.

• Monte Carlo tools (not discussed) are essential in the design phase. While EM simulations give satisfactory results, hadronic packages (GEANT4) still need improvements before being usable for LHC physics.
• Electromagnetic calorimeters are detectors difficult to build: high precision, high granularity has a technical cost.
• Located downstream of tracking devices, calorimeters suffer from the associated material: attempts being made to combine information from both detectors (converted photons, energy flow,..) need to be pursued.
• With the construction now in full swing, calorimeter teams are making every effort to stay on schedule. Still, they have to stay prepared for unexpected problems, both technical and financial...

Acknowledgements

All what was presented comes from the hard work of several hundreds of physicists, engineers and technical staff engaged since years in LHC calorimeters development and construction. They deserve warm thanks. To prepare the talk I benefited of discussions and information from many colleagues, and in particular Ph. Bloch, F. Gianotti, D. Green, P. Loch, C. Seez and L. Serin.

Finally I would like to thank the organisers of CALOR2002 for a well balanced program and many extremely interesting presentations.

Without the help of C. Bourge and C. Drouet, writing these proceedings (almost) in time would not have been possible: many thanks.

References

[1] ATLAS Liquid Argon Calorimeter Technical Design Report CERN/LHCC/96-41 dec 1996

[2] ATLAS Calorimeter Performance Technical Design Report CERN/LHCC/96-40 dec 1996

[3] Performance of a large scale prototype of the ATLAS accordion electromagnetic calorimeter. D.M. Gingrich et al., NIM A364(1995)290.

[4] Performance of the ATLAS Electromagnetic Calorimeter barrel module 0. To be submitted to NIM.

Performance of the ATLAS Electromagnetic Calorimeter end-cap module 0. To be submitted to NIM.

[5] CMS electromagnetic Calorimeter Technical Design Report CERN/LHCC/97-33 dec 1997

[6] The lead Tungstate Electromagnetic Calorimeter for CMS. R.Brown in Proceedings of CALOR 2000. Frascati Physics series number 21, 2001.

[7] CMS Note 2001/034 and C. Seez, private communication.

[8] ATLAS Inner Detector Technical Design Report CERN/LHCC/97-16 apr 1997, and updates.

[9] ATLAS Detector and Physics Performance Technical Design Report CERN/LHCC/99-14 may 1999, Vol I.

[10] CMS ECAL calibration Strategy. Imperial College workshop, Jan 2002.

[11] G.Unal for the NA48 Collaboration, in Proceedings of the 9th International Conference on Calorimetry, CALOR2000, Frascati Physics series, Vol 21,2001.

[12] LHCC - March 2002

[13] P. Paganini. Zero suppression in CMS. Presentation to this Conference.

[14] CMS hadron Calorimeter Technical Design Report CERN/LHCC/97-31 june 1997

[15] ATLAS Tile Calorimeter Technical Design Report CERN/LHCC/96-42 dec 1996

[16] Studies of the response of the prototype CMS hadron Calorimeter. V.V. Abramonov et al, NIMA 457, 475 (2001)

[17] Results of a new combined test of an EM Liquid argon calorimeter with a hadronic scintillating tile calorimeter.ATLAS Collaboration.S.Akhmadaliev et al NIMA 449, 461 (2000)

[18] D.Green Energy Flow in CMS (Sept 2001) and private communication.

[19] ATLAS Detector and Physics Performance Technical Design Report CERN/LHCC/99-14 may 1999, Vol II

[20] - Test beam of CMS quartz fibre prototype. N. Akchurin et al NIM A409 (1998) 593-597.
- Status of CMS HF Quartz Fiber Calorimetry. Y. Onel. Presentation to this conference.

[21] Forward Tagging and Jet Veto studies for Higgs events produced via Vector Boson Fusion. V. Cavasinni et al. ATLAS-PHYS-2002-008

[22] LHCb Technical Proposal CERN/LHCC/98-4

[23] ALICE Technical Proposal CERN/LHCC/95-71

[24] ALICE PHOS Technical Design Report CERN/LHCC/99-4

[25] ALICE ZDC Technical Design Report CERN/LHCC/99-5